Applied Catalysis B: Environmental 168-169 (2015) 353–362

Contents lists available at ScienceDirect

Applied Catalysis B: Environmental

journal homepage: www.elsevier.com/locate/apcatb

Greener synthesis of dimethyl carbonate using a novel ceria–zirconia oxide/graphene nanocomposite catalyst

Rim Saada[a], Suela Kellici[a], Tobias Heil[b], David Morgan[c], Basudeb Saha[a,*]

[a] Centre for Green Process Engineering, School of Engineering, London South Bank University, 103 Borough Road, London, SE1 0AA, UK
[b] Nanoinvestigation Centre at Liverpool, 1-3 Brownlow Street, Liverpool, L69 3GL, UK
[c] Cardiff Catalysis Institute, School of Chemistry, Cardiff University, Park Place Cardiff, CF10 3AT, UK

ARTICLE INFO

Article history:
Received 30 September 2014
Received in revised form 4 December 2014
Accepted 8 December 2014
Available online 12 December 2014

Keywords:
Carbon dioxide utilization
Dimethyl carbonate
Methanol
Ceria–zirconia oxide/graphene nanocomposite
Heterogeneous catalyst

ABSTRACT

A green, rapid and continuous hydrothermal flow synthesis (CHFS) route has been used to produce highly stable and active novel ceria–zirconia oxide/graphene nanocomposite catalyst [Ce–Zr oxide/graphene, where nominal atomic ratio of Ce:Zr (1:1)]. This catalyst has been investigated for the direct synthesis of dimethyl carbonate (DMC) from methanol (MeOH) and carbon dioxide (CO_2) using 1,1,1, trimethoxymethane (TMM) as a dehydrating agent in a high pressure reactor. The resulting graphene nanocomposites have been further subjected to heat treatment at 973 K for four hours in nitrogen. The as-prepared and the corresponding heat treated catalysts have been extensively characterized using powder X-ray diffraction (XRD), transmission electron microscopy (TEM), Brunauer–Emmett–Teller (BET) surface area measurement and X-ray photoelectron spectroscopy (XPS) analysis. The effect of various reaction conditions, such as reaction temperature, CO_2 pressure, catalyst loading and reaction time has been extensively evaluated. The optimum condition for the direct synthesis of DMC has been found at 383 K, 275 bar and 10% (w/w) catalyst loading. The ceria–zirconia oxide (Ce–Zr oxide)/graphene nanocomposite catalyst showed highest MeOH conversion of 58% at a DMC yield of 33%. Catalyst reusability studies have been conducted at optimum reaction condition and it has been found that this catalyst could be reused several times without losing its catalytic activity. These experimental findings indicated that novel ceria–zirconia oxide/graphene nanocomposite has a huge potential as a heterogeneous catalyst for the synthesis of DMC. The results also confirmed that the use of TMM markedly improved the conversion of MeOH and the yield of DMC.

1. Introduction

Carbon dioxide (CO_2) is the most important anthropogenic greenhouse gas; and therefore, it is considered as the main contributor for global warming. The conversion of CO_2 into value added chemicals has been widely investigated in an attempt to reduce the atmospheric levels of CO_2. Recently, CO_2 has attracted great interests as an environmentally benign building block in the chemical industry due to its non-toxic, non-flammable and recyclable properties [1–4]. However, CO_2 is a very stable compound as the carbon atom is in the most oxidized form and thermodynamically stable [5]; and therefore, large energy input is required to transform CO_2.

Dimethyl carbonate (DMC) is a promising environmentally benign compound that exhibits versatile and excellent chemical properties. It has low toxicity and high biodegradability which makes it a green reagent and a safer alternative to poisonous dimethyl sulphate and phosgene. It can be used as a good precursor material for the production of polycarbonates [6,7]. DMC's molec-

Abbreviations: CHFS, continuous hydrothermal flow synthesis; DMC, dimethyl carbonate; MeOH, methanol; CO_2, carbon dioxide; TMM, 1,1.1, trimethoxymethane; XRD, X-ray powder diffraction; TEM, transmission electron microscopy; sc-H_2O, supercritical water; BET, Brunauer–Emmett–Teller; XPS, X-ray photoelectron spectroscopy; GC, gas chromatograpghy; H_2O, water; CeO_2, cerium oxide; ZrO_2, zirconium oxide; V_2O_5, vanadium oxide; TiO_2, titanium oxide; SnO_2, tin oxide; GO, graphene oxide; IPA, isopropyl alcohol; $ZrO(NO_3)_2{\cdot}6H_2O$, zirconium(IV) oxynitrate; HCl, hydrochloric acid (HCl); H_2SO_4, sulfuric acid; NGP, natural graphite powder; $NaNO_3$, sodium nitrate; $Ce(NO_3)_3{\cdot}6H_2O$, cerium(III) nitrate hexahydrate; H_2O_2, hydrogen peroxide; KOH, potassium hydroxide pellets; $KMnO_4$, potassium permanganate; Ce–Zr oxide/graphene, ceria–zirconia graphene; HPLC, high performance liquid chromatography; HTR, catalyst prepared using hydrothermal reactor; HTR700, catalyst prepared using hydrothermal reactor and heat treated at 700 °C; CM, catalyst prepared using conventional wet impregnation method; CM700, catalyst prepared using conventional wet impregnation method and heat treated at 700 °C; FID, flame ionization detector.

* Corresponding author. Tel.: +44 2078157190; fax: +44 20 7815 7699.
E-mail address: b.saha@lsbu.ac.uk (B. Saha).

http://dx.doi.org/10.1016/j.apcatb.2014.12.013
0926-3373/

ular structure, which contains methyl, carbonyl and methoxyl active groups, makes it an important carbonylation and methylation agent. DMC has a high oxygen content (53%) and hence it can also be used as an oxygenate additive to gasoline to improve its performance and reducing exhaust emission [8].

Several reaction routes have been attempted for DMC production, including methanolysis of phosgene, oxidative carbonylation of methanol, transesterification route and direct synthesis from MeOH and CO_2 [6,9]. The latter being the most attractive route due to the inexpensive raw material and the avoidance of corrosive reagents, such as phosgene and dimethyl sulphate. The direct synthesis of DMC from MeOH and CO_2 has gained much interest recently.

Various catalysts have been studied extensively; however, methanol conversion and DMC yield are still very low. This is due to the equilibrium limited reaction (see Fig. 1) and the catalyst deactivation when water is formed as a by-product. Different dehydrating agents and additives have been used to minimize the effect of water produced during the reaction and improving the catalytic performance of the catalyst. These systems can be classified as reactive or non-reactive dehydration systems [10]. These agents include nitrile compounds [11,12], calcium chloride [13], 2,2-dimethoxy propane [14,15], molecular sieves [16], ketals [17], aldols [18] and trimethoxymethane (TMM) [8] and have positively contributed to increase MeOH conversion.

A variety of metal oxide catalysts has been developed and assessed for the effective synthesis of DMC. Cerium oxide (CeO_2) [19–24], zirconium oxide (ZrO_2) [19,25–30], vanadium oxide (V_2O_5) [13,31], titanium oxide (TiO_2) [32] and tin oxide (SnO_2) [26] have been investigated over the past few years in an attempt to maximize the catalytic performance and enhancing the production rate of DMC.

The usage of a support can increase the stability of the catalyst, optimize the dispersion of the active components of the catalyst, and provide important chemical, mechanical, thermal and morphological properties [33]. The general procedure for preparation of supported catalysts involve the transformation of the precursors into the required active compound and the deposition of the active compound onto the support surface. Different materials have been widely used as suitable catalyst supports in recent studies; these include silica [34,35], molecular sieve [36], complex supports [31], metal oxides [37], graphene oxide (GO), activated carbon and multi-walled carbon nanotubes [38].

Although there has been a considerable effort dedicated to the use of various metals as suitable catalysts, there is still a lack in finding suitable supports for the catalytic system and this area needs to be explored more [6,38]. As such, strongly coupled graphene based inorganic nanocomposites represent an exciting and new class of functional materials [39]. Unlike other carbon forms, graphene is a unique two-dimensional single layer of carbon in which the atoms are arranged in hexagons [40–42]. Its unique physical, chemical and mechanical properties including a very high surface area and easy surface modifications allow preparation of nanocomposite materials with novel properties and characteristics [43–45]. The current methods for homogeneously producing graphene-nanocomposites involve homogenization by mixing of inorganic nanoparticles and

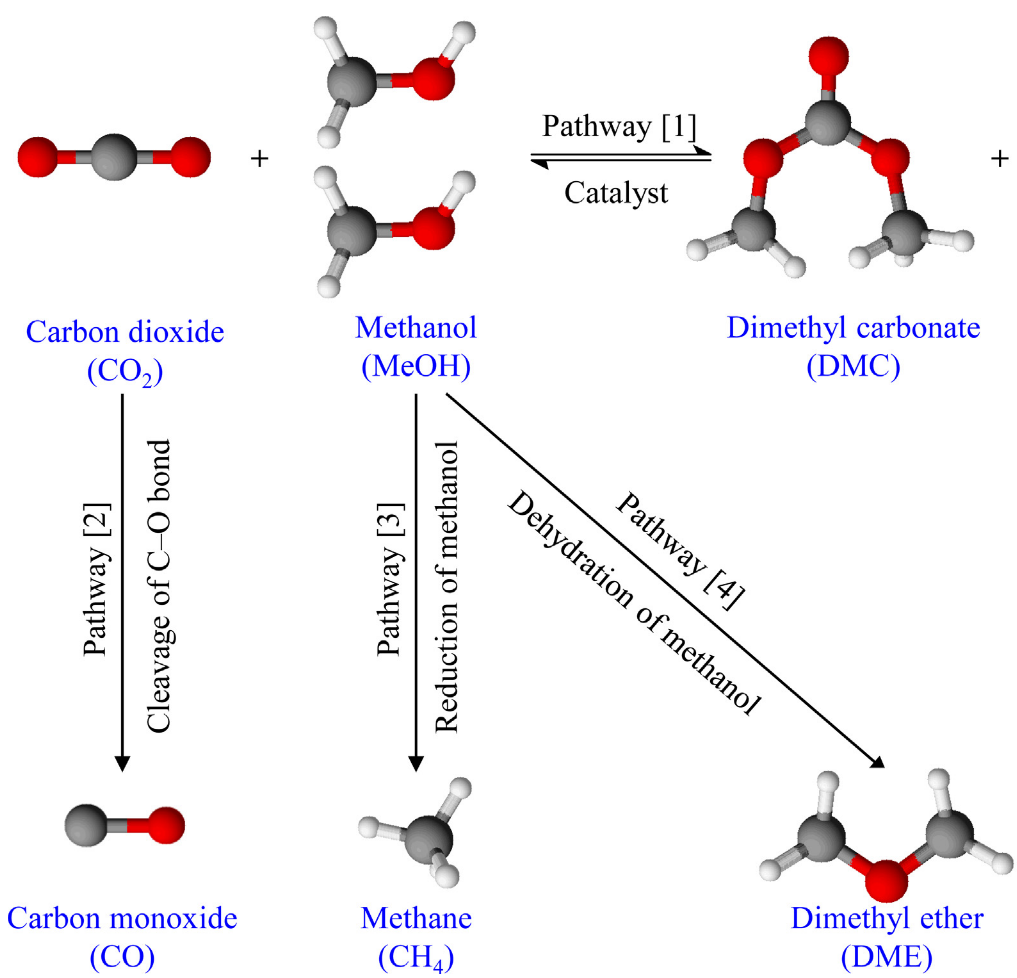

Fig. 1. Reaction scheme for the synthesis of DMC from MeOH and CO_2.

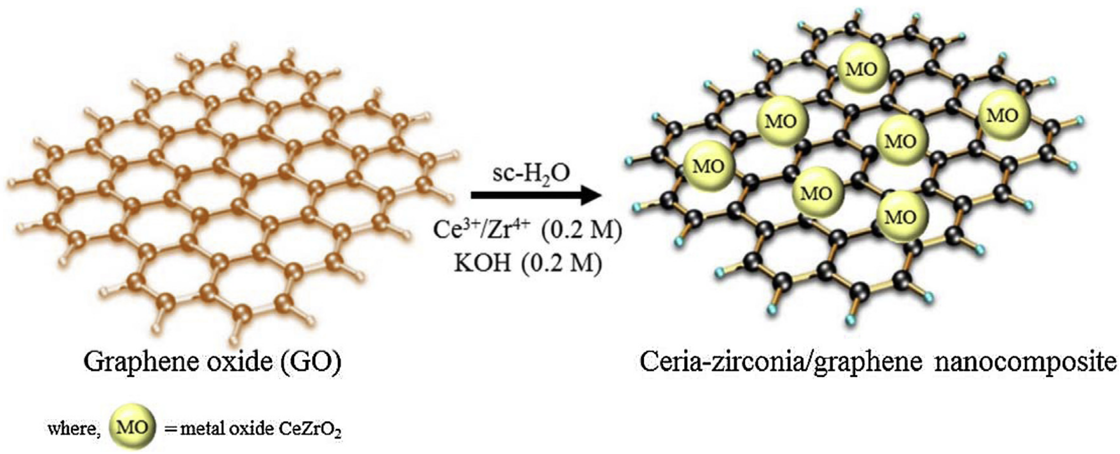

Fig. 2. A schematic representation of the synthesized Ce–Zr oxide/graphene nanocomposite catalyst.

grinding, which makes it extremely difficult to get very well dispersed nanoparticles in good electrical contact with the graphene. Thus, better bottom-up approaches are required. In the synthesis of metal oxides (homo, hetero or doped), hydrothermal syntheses in superheated or supercritical water can offer many advantages over conventional preparative methods including fewer synthetic steps and significantly faster reaction times [46–51]. There are currently very few scientific reports utilizing hydrothermal routes for decorating graphene with nanoparticles [52–55]. However, the current hydrothermal syntheses are conducted in batch reactors, which are time consuming and give little control over product properties such as crystallinity, size, *etc*. Continuous hydrothermal flow synthesis (CHFS) reactors offer many advantages as they have independent control over reaction variables (*e.g*., pressure and temperature) and hence particle properties [56,57]. Generally, the CHFS process involves mixing a flow of supercritical water with a flow of aqueous metal salt(s) to give rapid precipitation and controlled growth of nanoparticles in a continuous manner. The properties of water (such as diffusivity, density, and dielectric constant) change dramatically around the critical temperature and pressure (374 °C, 22.1 MPa) leading to its use as an exotic, and tunable reaction solvent/medium. As graphene has a very 2D, platelike structure, it offers an attractive substrate for deposition of inorganic nanoparticles for highly dispersed composites with novel properties.

In this work, an innovative approach has been employed for synthesizing advanced graphene-inorganic nanocomposite catalyst *via* utilization of a CHFS reactor. The catalytic activities of the as-synthesized materials have been tested using a new, greener and sustainable process for the direct synthesis of DMC from MeOH and CO_2. The use of 1,1,1-trimethoxymethane as a dehydrating agent has been evaluated. The optimum reaction conditions for the direct synthesis of DMC have been delineated.

2. Experimental

2.1. Materials

Methanol (MeOH), isopropyl alcohol (IPA) and dimethyl carbonate (DMC), 1,1,1-trimethoxymethane (TMM) and zirconium(IV) oxynitrate hydrate ($ZrO(NO_3)_2 \cdot 6H_2O$) were all purchased from Sigma–Aldrich (UK). Other chemicals were purchased from Fisher Scientific, UK, including hydrochloric acid (HCl), sulfuric acid (H_2SO_4), natural graphite powder (NPG), sodium nitrate ($NaNO_3$), cerium(III) nitrate hexahydrate ($Ce(NO_3)_3 \cdot 6H_2O$), hydrogen peroxide (H_2O_2), potassium hydroxide pellets (KOH) and potassium permanganate ($KMnO_4$). The liquid CO_2 cylinder (99.9%) equipped with a dip tube was purchased from BOC Ltd., UK.

2.2. Catalyst preparation

2.2.1. Preparation of graphene oxide

Natural graphite powder (NGP) was used as a precursor without any prior treatment. Recent modifications were made to the Hummer's method [58] for the synthesis of graphene oxide (GO) from NGP [59,60]. These modifications were adapted to synthesize graphene oxide. The synthesized GO was then used as a precursor for the synthesis of ceria–zirconia oxide/graphene nanocomposites [Ce–Zr oxide/graphene, where nominal atomic ratio of Ce:Zr (1:1)] prepared *via* CHFS and conventional method (wet impregnation) routes as shown in Fig. 2.

2.2.2. Ceria–zirconia oxide/graphene nanocomposite synthesis via conventional method

A control reaction using a traditional wet impregnation method was also conducted for the synthesis of Ce–Zr oxide/graphene nanocomposite catalyst. Cerium(III) nitrate hexahydrate ($Ce(NO_3)_3 \cdot 6H_2O$) and zirconium(IV) oxynitrate hydrate ($ZrO(NO_3)_2 \cdot 6H_2O$) were used as metal precursors. 1 g of GO was dispersed in 50 mL of deionized water by ultrasonic vibration for 1 h. The mixture was removed from the ultrasonic bath and 0.1882 g of $Ce(NO_3)_3 \cdot 6H_2O$ and 0.1 g of $ZrO(NO_3)_2 \cdot 6H_2O$ were added to the GO suspension and continuously stirred using a magnetic stirrer for 10 min. 6 mL of 8 M sodium hydroxide (NaOH) solution was added dropwise to the mixture while maintaining a vigorous agitation. The mixture was heated at 80 °C using an oil bath for 1 h and was then cooled down to room temperature. Ce–Zr/graphene nanocomposite catalyst was separated using a centrifuge (5000 rpm, 30 min per cycle). The prepared catalyst was washed twice with deionized water and dried at 40 °C for 24 h. The dried Ce–Zr/graphene nanocomposite catalyst was heat treated at different temperatures (*i.e*., 500 °C, 700 °C, 900 °C) under nitrogen for 4 h. The catalyst was cooled down for 4 h before it was used for testing. The samples synthesized *via* this method were labeled as CM.

2.2.3. Ceria–zirconia oxide/graphene nanocomposite synthesis via CHFS route

CHFS experiments were conducted using a reactor, basic design of which has been reported previously [47,61–63]. Briefly, the system consists of three high performance liquid chromatography (HPLC) pumps used for the delivery of aqueous solution of reagents as shown in Fig. 3. The tubing and fittings were 1/8 inch 316 SS Swagelok, except the counter-current reactor and the cooler, which were constructed using 1/4 inch fittings. Pump 1 (Gilson 307 fitted with 25 mL pump head) was utilized for delivering deionized water

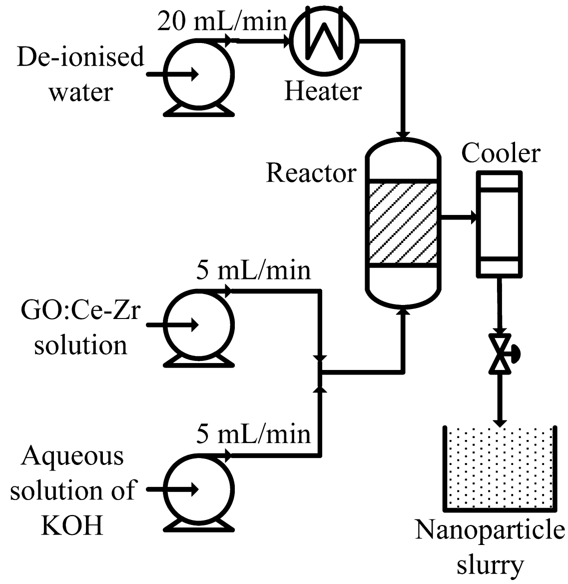

Fig. 3. Schematic of a CHFS reactor set-up used for the synthesis of Ce–Zr oxide/graphene nanocomposite catalyst.

through a custom made electrically powered pre-heater (2.5 kW) at a flow rate of 20 mL min^{-1}. Pumps 2 and 3 (Varian Pro Star 210 fitted with 5 mL pump head) were employed for pumping pre-sonicated aqueous GO solution premixed with corresponding cerium and zirconium salts at the desired ratios and KOH, respectively, at a flow rate of 5 mL min^{-1}. In a typical experiment, each pre-mixed aqueous solution of $Ce(NO_3)_3{\cdot}6H_2O$ and $ZrO(NO_3)_2{\cdot}6H_2O$ (with a total metal ion concentration of 0.2 M) and a pre-sonicated (30 min) aqueous solution of GO (4 μg mL^{-1}) were pumped to meet a flow of KOH (0.2 M) at a T-junction (see Fig. 3). The molar ratio of Ce^{3+}/Zr^{4+} = 1 and GO = 2. This mixture then meet superheated water (450 °C, 24.1 MPa) inside an in-house built 1/4 inch counter-current reactor whereupon the formation of ceria–zirconia oxide/graphene nanocomposite occurs in a continuous manner [49]. The aqueous suspension was cooled through a vertical cooler and the slurries were collected from the exit of the back pressure regulator. After collection, the particles were centrifuged and washed twice with deionized water. The solids were then freeze–dried. The dried catalyst was heat treated in a furnace under nitrogen at desired temperature for 4 h. The samples synthesized *via* CHFS route were identified as hydrothermal reactor (HTR).

2.3. Addition reaction of methanol and CO_2

The reaction for direct synthesis of dimethyl carbonate was carried out in a 25 mL stainless steel high pressure reactor (model 4590, Parr Instrument Company, USA) equipped with a stirrer, thermocouple (type J) and a heating mantle and controller (model 4848). 10 g of methanol were added to a ceria–zirconia oxide/graphene catalyst in a typical process. The reactor was heated to the required temperature and continuously stirred. Supercritical fluid pump (model SFT-10, Analytix Ltd., U.K) was used to pump CO_2 at a specified pressure from the cylinder to the reactor. CO_2 was injected at a constant pressure for all the optimized reactions. After the reaction, the reactor was cooled down to room temperature using an ice bath. The reactor was depressurized and the reaction mixture was filtered. The products were analyzed using a gas chromatography (GC) equipped with a flame ionization detector (FID) with a capillary column using isopropyl alcohol as an internal standard.

2.4. Catalyst characterization techniques

Particle size and morphology of as-prepared and heat treated graphene nanocomposites were investigated using a JEOL 2100FCs with a Schottky Field Emission Gun transmission electron microscope (200 kV accelerating voltage). Samples were collected on carbon-coated copper grids (Holey Carbon Film, 300 mesh Cu, Agar Scientific, Essex, UK) after being briefly dispersed ultrasonically in water. Particle size analysis was performed using ImageJ particle size analysis software. Brunauer–Emmett–Teller (BET) surface area measurements were performed on a Micromeritics Gemini VII analyzer (nitrogen adsorption and desorption method). The pore size distribution and pore volume were obtained using the Barrett–Joyner–Halenda (BJH) method. The powders were degassed at 573 K in N_2 (purge gas supplied by BOC, UK) for 5 h, prior to BET analysis. X-ray powder diffraction data were collected on a Panalytical X'pert Pro diffractometer with a X'celerator RTMS detector and an X-ray tube with a nickel filtered copper target (CuKa lambda = 0.15418 nm) set at 45 kV and 40 mA. The diffractograms were collected over a range from 5 to 70 degrees 2θ with a stepwidth of 0.0334 degrees and a collection time equivalent to 200 s per point and an incident beam divergence of 0.25 degrees. XPS measurements were performed using a Kratos Axis ultra DLD photoelectron spectrometer utilizing monochromatic Alka source operating at 144 W. Samples were mounted using conductive carbon tape. Survey and narrow scans were performed at constant pass energies of 160 and 40 eV, respectively. The base pressure of the system is *ca.* 1×10^{-9} Torr, rising to *ca.* 4×10^{-9} Torr under analysis of these samples.

2.5. Method of analysis

A Shimadzu gas chromatography (GC) was used for the separation and identification of experimental samples. The GC was equipped with a flame ionization detector (FID) and a capillary column. Helium was used as the carrier gas and was maintained at a flow rate of 1 mL min^{-1}. Oxygen and hydrogen were used as ignition gases. The detector and injector temperatures were maintained at 523 K. A spilt ratio of 25:1 and injection volume of 0.5 μL were chosen as part of the GC method. A ramp method was used to separate all the compounds present in the sample mixture where the initial temperature of the oven was set at 323 K. The sample was injected by an auto injector for analysis. The oven temperature was programmed at 323 K for 5 min after the sample had been injected. The oven temperature was ramped from 323 K to 523 K at the rate of 50 K min^{-1}. The total run time for each sample was 12 min. After each sample run, the oven temperature was cooled down to 313 K so that the following sample could be analyzed.

3. Results and discussion

3.1. Catalyst characterization

In this work, an innovative synthetic approach was employed for synthesizing nanoparticle functionalized graphene oxide *via* utilization of continuous flow of supercritical water in alkaline medium in a single rapid route. The Ce–Zr oxide/graphene nanocomposites were made from a 0.2 M (total concentration) pre-mixed aqueous solution of cerium and zirconium (to produce Ce^{3+}:Zr^{4+} at 50:50 atomic ratio) and GO (synthesized *via* conventional Hummers method) under alkaline conditions (KOH, 0.2 M). For comparison purposes, Ce–Zr oxide/graphene nanocomposite catalyst was also synthesized using a traditional wet impregnation method. Transmission electron microscopy (TEM) images of the as-prepared and heat treated materials are shown in Fig. 4 and the

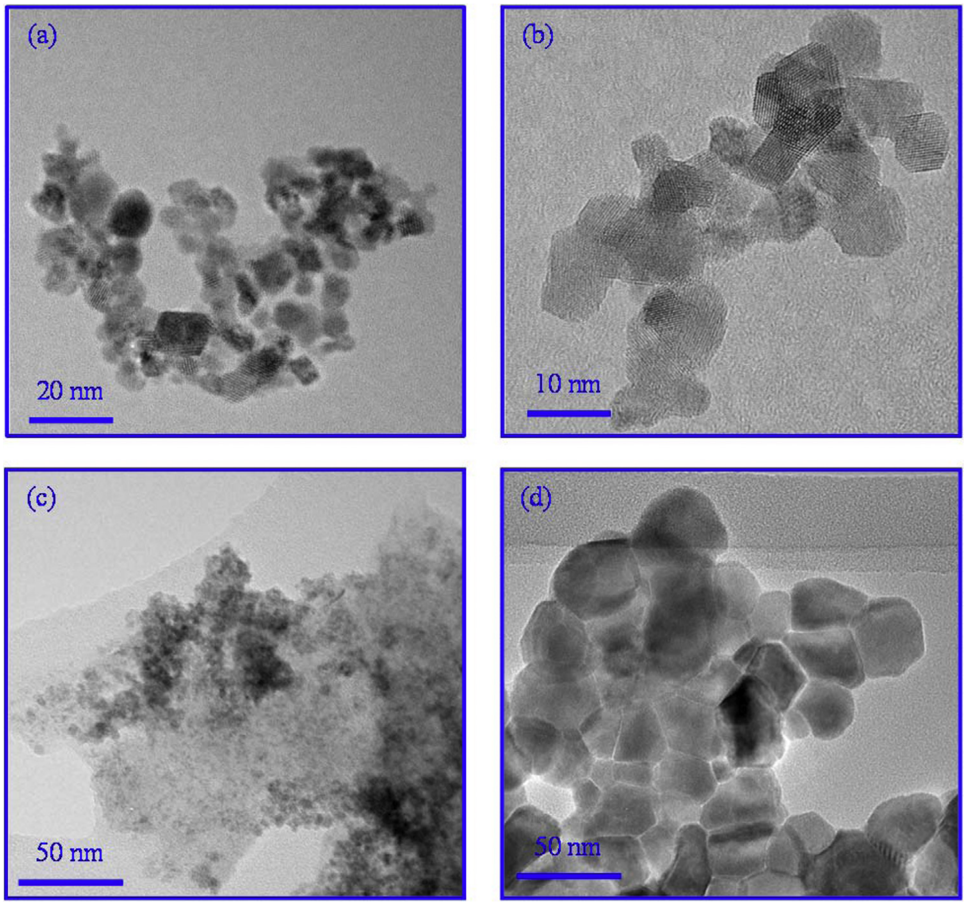

Fig. 4. Transmission electron microscopy (TEM) images of Ce–Zr oxide/graphene nanocomposite samples: (a) as-prepared sample synthesized using CHFS route labeled as HTR and (b) the corresponding heat-treated (700 °C) sample labeled as HTR700; (c) sample CM synthesized *via* wet impregnation route and (d) the corresponding heat treated (700 °C) sample labeled as CM700.

mean particle size values are given in Table 1. TEM images for Ce–Zr oxide/graphene synthesized using CHFS route (sample labeled as "HTR") revealed uniform particles exhibiting a mean particle size of 4.0 ± 1.1 nm (Fig. 4(a)). The TEM images for the corresponding heat treated sample at 700 °C (labeled as sample HTR700) showed an increase in particle size with a mean size of 5.8 ± 1.6 nm (Fig. 4(b)). By contrast, the TEM images (Fig. 4(c)) of the sample prepared *via* wet impregnation route (labeled as sample CM) exhibited undefined large agglomerated particles and particle size determination was proved to be challenging. In contrary, the corresponding heat treated Ce–Zr oxide/graphene sample revealed the largest mean crystallite size of 26.0 ± 8.5 nm. The crystallinity of the synthesized and heat treated at 700 °C Ce–Zr oxide/graphene nanocomposite catalysts synthesized *via* CHFS and conventional wet impregnation route was assessed by X-ray powder diffraction (XRD) and is shown in Fig. 5.

The XRD pattern for the sample synthesized *via* CHFS route (HTR sample) gave very broad peaks corresponding to the fluorite structure, suggesting the formation of the solid solution. It has been reported that as the zirconium concentration in the solid solutions increases, the positions of the CeO_2 diffraction peaks shift to higher 2θ values, corresponding to a decrease in the lattice parameter. The observed lattice cell shrinkage is caused by the insertion of smaller Zr^{4+} ions into the ceria fluorite, Ce^{4+} lattice [64–66]. Furthermore, there is no change in the pattern for the corresponding heat treated sample (HTR700) indicating the thermal stability and high homogeneity of the compound synthesized under CHFS condition. The peak broadness of the observed reflections is reported to be due

Table 1
Physical and chemical properties of Ce–Zr oxide/graphene nanocomposite catalysts.

Catalyst properties	Catalysts			
	HTR	HTR700	CM	CM700
BET surface area ($m^2\,g^{-1}$)	167	106	2	11
BJH adsorption average pore diameter (nm)	4.9	6.7	4.9	7.3
TEM particle size (nm)	4.0 ± 1.1	5.8 ± 1.6	Large agglomerates	26 ± 8.5
Atomic concentration (%) (by XPS analysis)	Ce 3d:8.74 O 1s: 35.43 C 1s: 48.73 Zr 3d: 7.11	Ce 3d:11.74 O 1s: 41.03 C 1s: 38.8 Zr 3d: 8.44	Ce 3d:0.38 O 1s: 21.33 C 1s: 71.61 Zr 3d: 0.63 Na 1s: 6.04	Ce 3d:5.19 O 1s: 45.85 C 1s: 24.74 Zr 3d: 4.81 Na 1s: 7.92 K 2s: 7.54 Cl 2s: 3.97

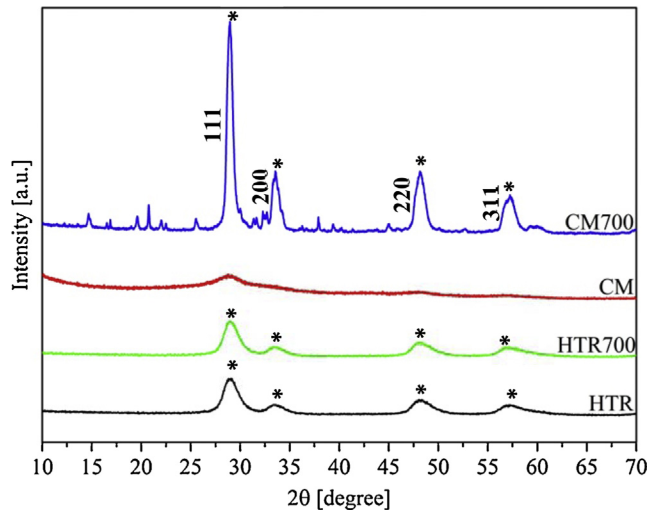

Fig. 5. X-ray powder diffraction (XRD) patterns of different ceria–zirconia oxide/graphene nanocomposites.
* = reflections assigned to fluorite structure.

to the small crystallite size [64], which is in good agreement with the particle size data obtained from TEM imaging. In contrast, the as-prepared sample synthesized *via* conventional method (sample CM) revealed an amorphous pattern, which is expected considering the synthetic process utilized for catalyst preparation. The corresponding heat treated sample (CM700) is a mixture of CeO_2 or Ce–Zr oxide/graphene, which provides broad peaks along with other unidentified peaks. For all cases, we did not observe peaks corresponding to GO.

To investigate the changes in the concentration of cerium and zirconium in the lattice, their oxidation states and the chemical states of graphene oxide for all synthesized and heat treated catalysts, X-ray photoelectron spectroscopy (XPS) analysis was employed and the spectra of which are shown in Fig. 6. The XPS elemental analysis for all catalysts *i.e.* as-prepared sample *via* CHFS (HTR), corresponding sample heat treated at 700 °C (HTR700), the as-prepared sample *via* conventional route (CM) and the corresponding sample heat treated at 700 °C (CM700) are given in Table 1. Generally, the spectra of all the samples showed strong peaks corresponding to cerium, zirconium, oxygen and carbon. For the conventionally synthesized sample, peaks for sodium were also observed. As previously reported in our paper [63] the hydrothermal process is effective in dehydrating/reducing GO. Indeed, the deconvoluted C(1s) XPS spectra of samples made hydrothermally revealed significant reduced peak intensities of the oxygen-containing functional groups (epoxide, carboxyl and hydroxyl), which are associated with GO (starting material). Furthermore, the XPS analysis revealed a complex spectrum for cerium indicating the presence of both Ce(IV) and Ce(III) species as evidenced by the peaks at *ca.* 916 eV (Ce(IV)) [67] and the intensity toward lower binding energy of the Ce(3d5/2) peak (*ca.* 880 eV), respectively. The calculation of the exact Ce(III)/Ce(IV) ratio is difficult, however, using the method employed by Preisler et al. [68] we have estimated the Ce(III) content to be approximately 10%. XPS spectrum of the Zr 3d core level has a strong spin–orbit doublet due to Zr 3d5/2 at 182.3 eV and Zr 3d3/2 at 184.7 eV with spin–orbit separation of 2.4 eV, which is in excellent agreement with reported literature values [69] and characteristic of Zr^{4+} ions in their full oxidation state.

Table 1 shows the BET specific surface area (SSA) of all as-prepared and heat treated catalysts synthesized *via* CHFS and wet impregnation route (as control reaction). It is to be noted that sample HTR shows the highest SSA (167 $m^2\,g^{-1}$), which decreased to 106 $m^2\,g^{-1}$ with heat treatment of the catalyst. This is attributed to an increase in the particle size of Ce–Zr oxide/graphene as confirmed from TEM data (Table 1). However, samples synthesized *via* conventional method, exhibited a very low SSA values (2 $m^2\,g^{-1}$ and 11 $m^2\,g^{-1}$ for CM and CM700, respectively). This is expected, given that the particle size of the CM700 (26 ± 8.5 nm) is larger than sample HTR700 (5.8 ± 1.6 nm).

It is known that both acidic and basic sites on the catalyst surface play an important role on DMC synthesis and greatly influence the activity and selectivity of the desired product [70–72]. In regards to the GO, it is to be noted that since carbon atoms do not have empty or full orbitals to act as base centers or Lewis acid, functionalization is considered as a suitable route for introduction of acidic or basic site [73]. Additionally, the acid–base properties of ceria–zirconia solid solutions and their corresponding parent metal oxides have been formerly investigated [74]. It has been reported that ceria exhibits the lowest strength of acid site, which increases upon addition of zirconia with pure zirconia exhibiting the highest value. In contrary, the ceria rich solid solutions reveal a high basic character. Generally, the introduction of high concentrations of zirconia into ceria lattice, were also associated with complex features on both basicity and acidity in comparison to the pure parent oxide [74]. Furthermore, is has been reported that weak acidity is favorable in DMC synthesis since the side product DME is produced on the strong acid sites.

3.2. *Batch experimental results*

Addition reactions of carbon dioxide (CO_2) to methanol (MeOH) were carried out at different reaction conditions in the presence of Ce–Zr oxide/graphene nanocomposite as catalysts. All addition reactions were conducted in the presence of 1,1,1-trimethylmethoxymethane (TMM) as a dehydrating agent. The effects of temperature, CO_2 pressure, reaction time, catalyst loading and TMM:MeOH mass ratio on the yield of DMC were studied. Reusability studies were conducted to evaluate the long term stability of Ce–Zr oxide/graphene catalyst for the synthesis of DMC.

The addition reaction of MeOH and CO_2 in the presence of a suitable heterogeneous catalyst produces a value added product, *i.e.* DMC along with other side products. The reaction scheme for the synthesis of DMC from MeOH and CO_2 is shown in Fig. 1. The expected side products from the addition reaction of MeOH and CO_2 in the presences of TMM include carbon monoxide (CO), methane (CH_4), dimethyl ether (DME), methyl methanoate and water (H_2O) [6,8,38,75] (see Fig. 1). CO can be produced as a result from the cleavage of the C—O bond of the CO_2, ethane can be produced upon reduction of methanol, DME comes from the dehydration of methanol and methyl methanoate is formed from the hydrolysis of TMM [6,8,38,75]. However, these by-products were below the limit of the GC-FID used in the analysis; and therefore, specific yields of the by-products were not calculated. This observation is similar to the work published by Zhang et al. [8].

3.2.1. *Effect of different catalysts*

The performance of various Ce–Zr oxide/graphene catalysts was assessed for the effective synthesis of DMC from the reaction of MeOH and CO_2 in the presence of TMM as shown in Fig. 7. Catalyst activity was indicated by methanol conversion and DMC yield, where two molecules of methanol are incorporated into DMC. CM and HTR represent Ce–Zr oxide/graphene catalyst synthesized using conventional method and CHFS method, respectively. The catalysts were heat treated at different temperatures (500–700 °C and 900 °C) to enhance their catalytic activity. When the catalyst was prepared using CM, the yield of DMC was low (3.9%) and increased when the catalyst was heat treated to 700 °C (22.7%). The

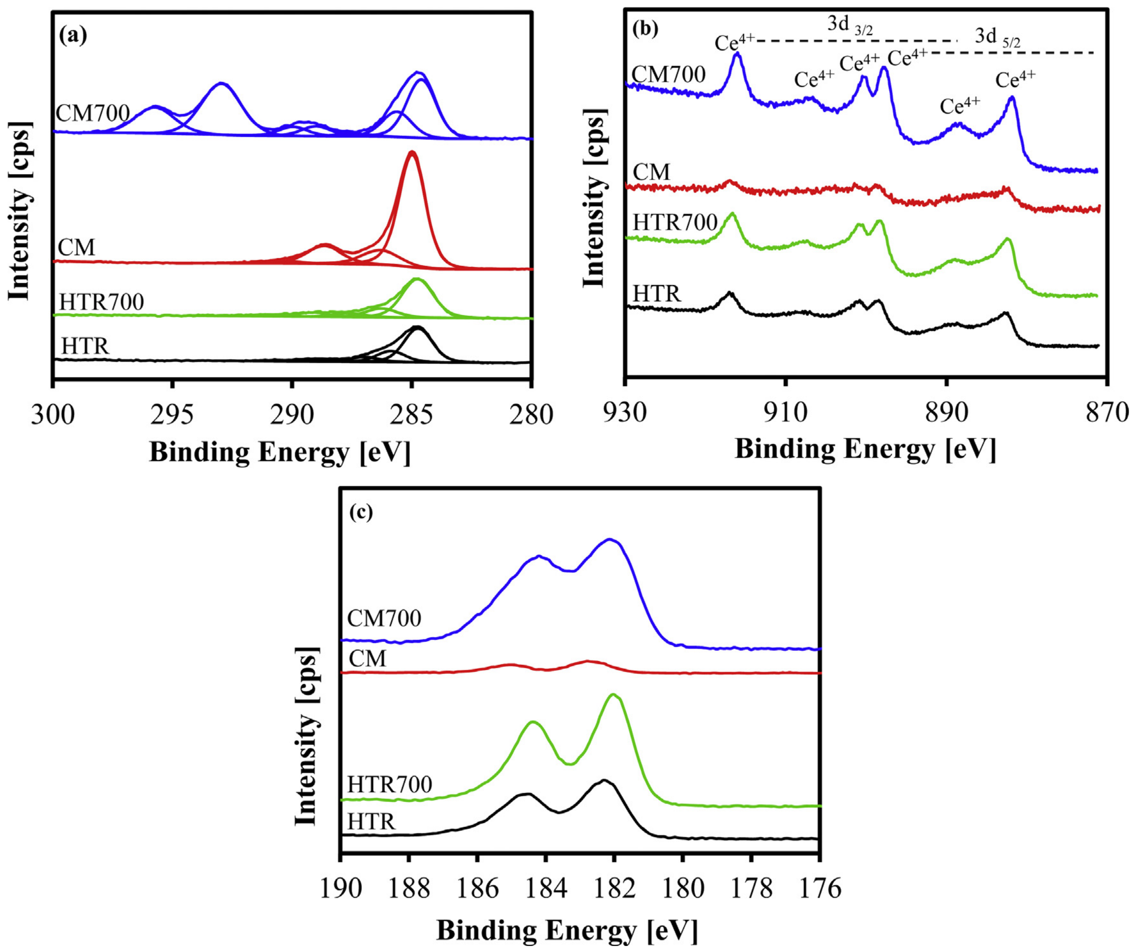

Fig. 6. X-ray photoelectron spectroscopy (XPS) spectra showing the (a) deconvoluted C(1s) (b) Ce(3d) region and (c) Zr (3d) region for of Ce–Zr oxide/graphene samples synthesized *via* continuous hydrothermal flow reactor and conventional wet impregnation route.

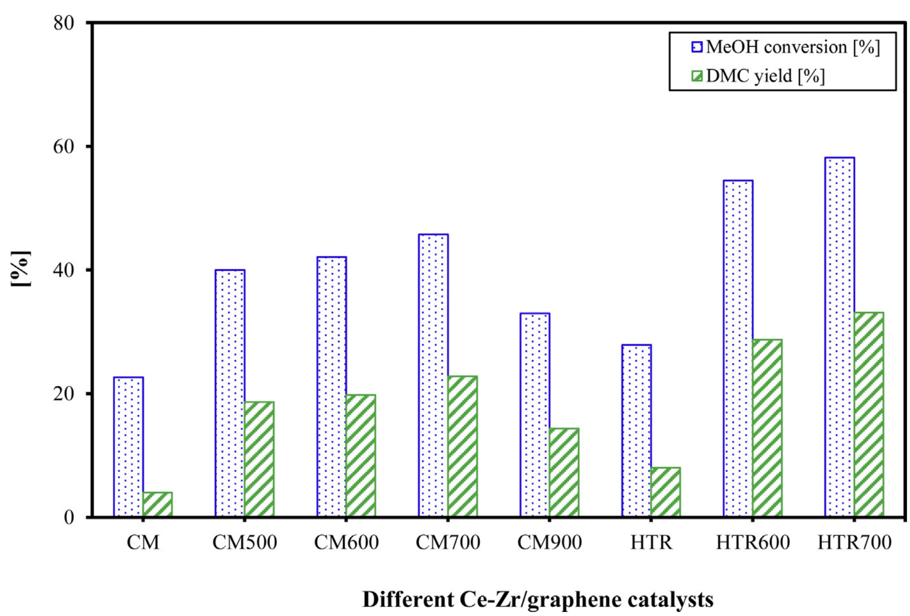

Fig. 7. Effect of different Ce–Zr oxide/graphene nonocomposite catalysts on the direct synthesis of DMC. Experimental conditions: MeOH:TMM 1:1(w/w); reaction temperature 383 K; CO_2 pressure 275 bar; reaction time 16 h and catalyst loading 10% (w/w).

activity of the catalyst synthesized using HTR showed a slightly better performance with a DMC yield of 7.9%. This DMC yield further increased to 33% when the catalyst (HTR700) was heat treated at 700 °C.

The study showed that the catalyst prepared using HTR had a higher catalytic activity to that prepared using CM. The differences in the catalytic performance can be attributed to a series of parameters including smaller particle size, phase composition, crystallinity and high surface area. From Fig. 7, it can be seen that Ce–Zr oxide/graphene catalyst prepared using CHFS and heat treated at 700 °C (HTR700) showed the highest activity with 58% conversion of MeOH and 33% yield of DMC. Based on this study, Ce–Zr oxide/graphene HTR700 was found to be the best catalyst for the synthesis of DMC and was used for further studies.

3.2.2. Effect of catalyst loading

The effect of catalyst loading (*i.e.* the percentage ratio of the mass of the catalyst to the mass of the limiting reactant, *i.e.*, MeOH) was investigated using 5%, 10% and 15% catalyst loading for the reaction of MeOH and CO_2 as shown in Fig. 8(a). It can be seen that an increase in catalyst loading (w/w) from 5% to 10% had increased MeOH conversion from 53.7% to 58% and the yield of DMC increased from 30.3% to 33%. However, a further increase in catalyst loading to 15% (w/w) has no obvious increase in the MeOH conversion and the yield of DMC. In view of the experimental error of ±3%, it seems that the number of active sites required for MeOH and CO_2 to react and produce DMC was sufficient at 10% (w/w) catalyst loading. Therefore, it was not necessary to increase the catalyst loading to 15% (w/w). Hence, it can be concluded that 10% (w/w) catalyst loading is the optimum amount of catalyst required for this reaction.

3.2.3. Effect of reaction temperature

The direct synthesis of DMC *via* the reaction of CO_2 and MeOH was carried out between temperature 373 K and 433 K in order to study the effect of reaction temperature on the yield of DMC. Fig. 8(b) presents the variation of MeOH conversion and DMC yield at different reaction temperatures. The conversion of MeOH was 59.5% and the yield of DMC was 31.8% at 393 K after 16 h; whereas, at 383 K MeOH conversion was 58% and the yield of DMC reached to 33%. Higher reaction temperatures gave higher conversion of MeOH at a fixed reaction time for the catalyzed reaction; however, the yield of DMC was decreased (see Fig. 8(b)).

At high temperatures, it is thermodynamically favorable for DMC to react with oxygen to form carbon dioxide and water. Other possible by products of DMC decomposition include carbon monoxide, methanol, formaldehyde, formic acid, and their reaction products [76]. During analysis, formaldehyde did not appear as a by-product. Other by-products were under the detection limit of the GC-FID used in the analysis. This observation is similar to the work published by Zhang et al. [8].

From this study it can be concluded that the optimum temperature for the endothermic reaction of MeOH and CO_2 using Ce–Zr oxide/graphene catalyst is 383 K. Similar reaction temperatures for the synthesis of DMC from MeOH and CO_2 have been reported in the literature [6,8,77].

3.2.4. Effect of CO_2 pressure

The pressure of CO_2 is an important reaction parameter for the addition reaction of MeOH and CO_2. Near critical or supercritical state CO_2 reaction system can cause an increase in the mass transfer efficiency of the reactants and shift the reaction equilibrium to break the thermodynamic limitation of this reaction [78]. The effect of CO_2 pressure on the MeOH conversion and DMC yield was studied in order to assess the optimum CO_2 pressure for the catalyzed reaction. The experiments were conducted in a high pressure reactor at 383 K within a pressure range of 120–290 bar for 16 h and the results are shown in Fig. 8(c). It can be seen from Fig. 8(c) that an increase in CO_2 pressure increases MeOH conversion and the yield of DMC. At a CO_2 pressure of 200 bar, MeOH conversion and yield of DMC were 47% and 28%, respectively. As the CO_2 pressure was further increased to 275 bar, MeOH conversion and yield of DMC increased to 58% and 33%, respectively. A further increase in pressure to 290 bar showed no significant increase in the methanol conversion or the yield of DMC (Fig. 8(c)). Therefore, from this study, it can be concluded that the optimum CO_2 reaction pressure is 275 bar.

This study shows that an increase in the reaction pressure increases methanol conversion due to an improvement of the physical properties of CO_2, such as polarity and solubility at supercritical conditions. Supercritical CO_2 have characteristics that affect the activation of the CO_2 molecule in catalytic reactions to the greatest extent [79]. It has been reported that proper use of supercritical CO_2 in heterogeneous catalysis provides a great enhancement of reaction rates and catalyst reusability [79–82]. Supercritical CO_2 helps to reduce mass and heat transfer limitations and avoids coke formation and catalyst poisoning [81]. During the reaction between MeOH and CO_2, there are two phases for the reaction mixture below supercritical conditions, whereas, there is only one phase at supercritical conditions. This favors the catalytic conversion of MeOH and CO_2 and shifts the reaction equilibrium to the product side enhancing the yield of DMC. Zhao et al. [77] had reported that near supercritical conditions, the yield of DMC was 12 times higher than that at non-supercritical conditions.

3.2.5. Effect of reaction time

The influence of varying the reaction time on the yield of DMC was studied by carrying out a set of addition reactions of MeOH to CO_2 in the presence of the best performed Ce–Zr oxide/graphene catalyst (HTR700) and the results are shown in Fig. 8(d). A MeOH conversion of 58% and DMC yield of 33% were achieved when the reaction was carried out for 16 h, which marginally increased to 58.2% and 33.1%, respectively, when the reaction was carried out for 20 h. These results clearly show that there has been no significant increase in the yield of DMC with prolonged reaction time, indicating that 16 h is the optimum reaction time for this catalyzed system.

3.2.6. Effect of dehydrating agent

In order to overcome the thermodynamic limitations of the reaction between MeOH and CO_2, TMM has been added to remove the water produced during the reaction. TMM can also react with CO_2 to produce DMC. Therefore, a blank run was carried out at optimum condition to that of DMC synthesis for the reaction between TMM and CO_2. The reaction between TMM and CO_2 in the presence of Ce–Zr oxide/graphene catalyst did not produce any DMC, which suggests that this catalyst is not selective for this particular reaction. This result agrees with the work published by Zhang et al. [8].

Direct synthesis of DMC was studied using different mass ratio of TMM to MeOH (TMM:MeOH) in the presence of HTR700 catalyst. It can be seen from Fig. 8(e) that the methanol conversion and yield of DMC increased from 50 to 58% and 25% to 33%, respectively, when TMM:MeOH increased from 0.25:1 to 1:1. There was no further increase in MeOH conversion or yield of DMC when TMM:MeOH increased to 2:1. From this study, it can be concluded that the addition of TMM enhances the conversion of MeOH and DMC yield by shifting the equilibrium to the right and that the optimum TMM:MeOH ratio is 1:1.

3.2.7. Catalyst reusability studies

The reusability of ceria–zirconia/graphene nanocomposites was studied by carrying out a set of experiments at the optimum

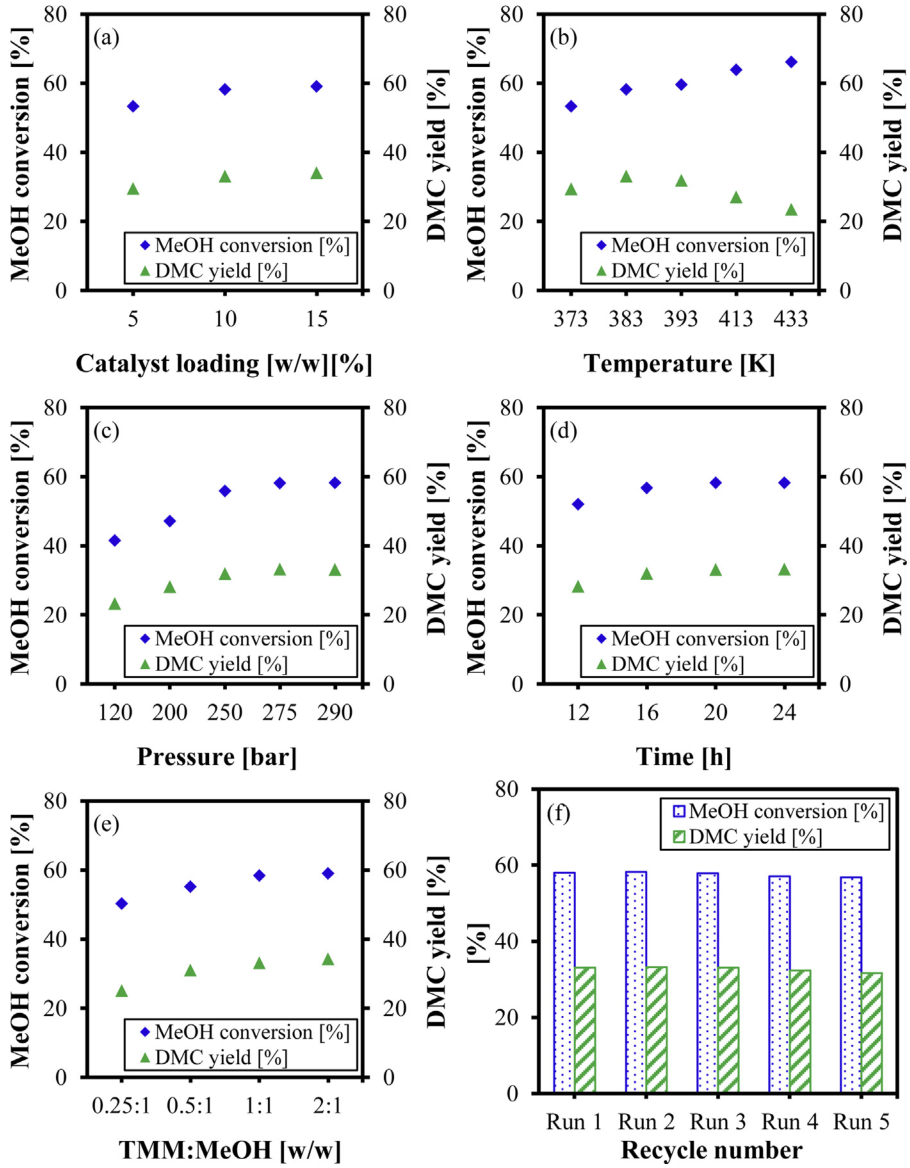

Fig. 8. Effect of (a) catalyst (Ce–Zr oxide/graphene nanocomposite) loading at 383 K, 275 bar, 1:1 TMM:MeOH (w/w) and 16 h; (b) reaction temperature at catalyst loading 10% (w/w), 275 bar, 1:1 TMM:MeOH (w/w) and 16 h; (c) CO_2 pressure at catalyst loading 10% (w/w), 383 K, 1:1 TMM:MeOH (w/w) and 16 h; (d) reaction time at catalyst loading 10% (w/w), 383 K, 275 bar and 1:1 TMM:MeOH (w/w); (e) TMM:MeOH mass ratio at catalyst loading 10% (w/w), 383 K, 275 bar and 16 h on MeOH conversion and DMC yield; (f) catalyst reusability studies at catalyst loading 10% (w/w), 383 K, 275 bar, 1:1 TMM:MeOH (w/w) and 16 h.

reaction condition obtained from the batch studies (*i.e.*, reaction temperature 383 K, CO_2 pressure 275 bar, 10% catalyst loading (w/w), 1:1 TMM:MeOH (w/w) and 16 h). The first reaction (labeled as run 1) was carried out using a fresh catalyst as shown in Fig. 8(f). The catalyst was recovered by filtration from the reaction mixture, washed twice with acetone and dried at 333 K for 12 h. The catalyst was then reused for subsequent experiments (labeled Run 2–6) under the same reaction conditions as shown in Fig. 8(f). It can be observed that MeOH conversion and yield of DMC remained comparable even after the 6th Run. It is evident that ceria–zirconia/graphene nanocomposites can be easily recovered and reused without any significant reduction in the catalytic performance.

4. Conclusions

The preparation of graphene by continuous hydrothermal flow synthesis route allowed simultaneously and homogeneously growing and dispersing metal oxide nanoparticles into graphene substrate in a single step. This single step synthetic approach not only enables control over oxidation state of graphene, but also offers an optimal route for homogeneously producing and depositing highly crystalline nanostructures into graphene oxide. The synthesized Ce–Zr oxide/graphene was successfully applied for the direct synthesis of DMC from MeOH and CO_2. The effect of various parameters such as the reaction time, reaction temperature, CO_2 pressure, catalyst loading and the addition of dehydrating agent was studied for the optimization of DMC synthesis. It was found that an increase in CO_2 pressure resulted in an increase in the MeOH conversion and yield of DMC. The experimental results revealed that the use of a dehydrating agent (TMM) to remove residual water produced during the reaction enhances yield of DMC. The highest MeOH conversion of 58% and DMC yield of 33% were obtained at an optimum reaction condition of 110 °C, 275 bar, 1:1(w/w) TMM:MeOH and 16 h using 10% (w/w) Ce–Zr oxide/graphene nanocomposite catalyst. The catalyst was easily

recycled and reused several times without any reduction in its catalytic performance.

Acknowledgments

Rim Saada gratefully acknowledges the financial support provided by London South Bank University. The authors are thankful to Dr. Dipesh Patel and Mr. Steve Jones for their support and help during this work.

References

[1] E. Leino, P. Mäki-Arvela, V. Eta, D.Y. Murzin, T. Salmi, J.P. Mikkola, Appl. Catal. A: Gen. 383 (2010) 1–13.
[2] Y. Dienes, W. Leitner, M.G.J. Müeller, W.K. Offermans, T. Reier, A. Reinholdt, T.E. Weirich, T.E. Müeller, Green Chem. 14 (2012) 1168–1177.
[3] A.I. Adeleye, D. Patel, D. Niyogi, B. Saha, Ind. Eng. Chem. Res. (2014), http://dx.doi.org/10.1021/ie500345z, In press.
[4] M. Honda, M. Tamura, K. Nakao, K. Suzuki, Y. Nakagawa, K. Tomishige, ACS Catal. 4 (2014) 1893–1896.
[5] I. Omae, Coord. Chem. Rev. 256 (2012) 1384–1405.
[6] J. Bian, M. Xiao, S. Wang, Y. Lu, Y. Meng, Catal. Commun. 10 (2009) 1142–1145.
[7] J. Bian, M. Xiao, S.J. Wang, Y.X. Lu, Y.Z. Meng, Chin. Chem. Lett. 20 (2009) 352–355.
[8] Z.F. Zhang, Z.W. Liu, J. Lu, Z.T. Lie, Ind. Eng. Chem. Res. 50 (2011) 198–1988.
[9] D. Ballivet-Tkatchenko, S. Chambrey, R. Keiski, R. Ligabue, L. Plasseraud, P. Richard, H. Turunen, Catal. Today 115 (2006) 80–87.
[10] M. Honda, M. Tamura, Y. Nakagawa, K. Tomishige, Catal. Sci. Technol. 4 (2014) 2830–2845.
[11] M. Honda, S. Kuno, N. Begum, K. Fujimoto, K. Suzuki, Y. Nakagawa, K. Tomishige, Catal. A: Gen. 384 (2010) 165–170.
[12] M. Honda, S. Kuno, S. Sonehara, K. Fujimoto, K. Suzuki, Y. Nakagawa, K. Tomishige, ChemCatChem 3 (2011) 365–370.
[13] X.L. Wu, M. Xiao, Y.Z. Meng, Y.X. Lu, J. Mol. Catal. A: Chem. 238 (2005) 158–162.
[14] K. Tomishige, K. Kunimori, Appl. Catal. A: Gen. 237 (2002) 103–109.
[15] M. Honda, A. Suzuki, N. Begum, K. Fujimoto, K. Suzuki, K. Tomishige, Chem. Commun. 4596 (2009) 4596–4598.
[16] Z.S. Hou, B.X. Han, Z.M. Liu, T. Jiang, G.Y. Yang, Green Chem. 4 (2002) 467–471.
[17] T. Sakakura, J.C. Choi, Y. Saito, T. Sako, Polyhedron 19 (2000) 573–576.
[18] T. Sakakura, J. Choi, H. Yasuda, Chem. Rev. 107 (2007) 2365–2387.
[19] K. Tomishige, Y. Furusawa, Y. Ikeda, M. Asadullah, K. Fujimoto, Catal. Lett. 76 (2001) 71–74.
[20] N.A.M. Razali, K.T. Lee, S. Bhatia, A.R. Mohamed, Renew. Sust. Energ. Rev. 16 (2012) 4951–4964.
[21] Y. Yoshida, Y. Arai, S. Kado, K. Kunimori, K. Tomishige, Catal. Today 115 (2006) 95–101.
[22] A. Bansode, A. Urakawa, ACS Catal. 4 (2014) 3877–3880.
[23] M. Honda, M. Tamura, Y. Nakagawa, K. Nakao, K. Suzuki, K. Tomishige, J. Catal. 318 (2014) 95–107.
[24] M. Honda, M. Tamura, Y. Nakagawa, S. Sonehara, K. Suzuki, K. Fujimoto, K. Tomishige, ChemSusChem 6 (2013) 1341–1344.
[25] K.T. Jung, A.T. Bell, J. Catal. 204 (2001) 339–347.
[26] D. Aymes, D. Ballivet-Tkatchenko, K. Jeyalakshmi, L. Saviot, S. Vasireddy, Catal. Today 147 (2009) 62–67.
[27] K. Tomishige, Y. Ikeda, T. Sakaihori, K. Fujimoto, J. Catal. 192 (2000) 355–362.
[28] Y. Ikeda, T. Sakaihori, K. Tomishige, K. Fujimoto, Catal. Lett. 66 (2000) 59–62.
[29] Y. Ikeda, M. Asadullah, K. Fujimoto, K. Tomishige, J. Phys. Chem. B 105 (2001) 10653–10658.
[30] K. Tomishige, T. Sakaihori, Y. Ikeda, K. Fujimoto, Catal. Lett. 58 (1999) 225–229.
[31] X.L. Wu, Y.Z. Meng, M. Xiao, Y.X. Lu, J. Mol. Catal. A: Chem. 249 (2006) 93–97.
[32] K.W. La, I.K. Song, React. Kinet Catal. Lett. 89 (2006) 303–309.
[33] H. Dai, J.H. Hafner, A.G. Rinzler, D.T. Colbert, R.E. Smalley, Nature 384 (1996) 147–150.
[34] D. Ballivet-Tkatchenko, F. Bernard, F. Demoisson, L. Plasseraud, S.R. Sanapureddy, ChemSusChem 4 (2011) 1316–1322.
[35] B. Fan, H. Li, W. Fan, J. Zhang, R. Li, Appl. Catal. A: Gen. 372 (2010) 94–102.
[36] H. Chen, S. Wang, M. Xiao, D. Han, Y. Lu, Y. Meng, Chin. J. Chem. Eng. 20 (2012) 906–913.
[37] K. Almusaiteer, Catal. Commun. 10 (2009) 1127–1131.
[38] J. Bian, M. Xiao, S.J. Wang, Y.X. Lu, Y.Z. Meng, J. Colloid Interface Sci. 334 (2009) 50–57.
[39] S. Bai, X. Shen, RSC Adv. 2 (2012) 64–98.
[40] A.K. Geim, K.S. Novoselov, Nat. Mater. 6 (2007) 183–191.
[41] A.K. Geim, Science 324 (2009) 1530–1534.
[42] C.N.R. Rao, A.K. Sood, K.S. Subrahmanyam, A. Govindaraj, Angew. Chem. Int. Ed. 48 (2009) 7752–7777.
[43] D.R. Dreyer, S. Park, C.W. Bielawski, R.S. Ruoff, Chem. Soc. Rev. 39 (2010) 228–240.
[44] D. Li, R.B. Kaner, Science 320 (2008) 1170–1171.
[45] G. Williams, B. Seger, P.V. Kamat, ACS Nano 2 (2008) 1487–1491.
[46] J.A. Darr, M. Poliakoff, Chem. Rev. 99 (1999) 495–541.
[47] A.A. Chaudhry, S. Haque, S. Kellici, P. Boldrin, I. Rehman, F.A. Khalid, J. Darr, Chem. Commun. 77 (21) (2006) 2286–2288, http://dx.doi.org/10.1039/b518102j.
[48] Y. Hakuta, T. Adschiri, T. Suzuki, T. Chida, K. Seino, K. Arai, J. Am. Ceram. Soc. 81 (1998) 2461–2464.
[49] E. Lester, P. Blood, J. Denyer, D. Giddings, B. Azzopardi, M. Poliakoff, J. Supercrit. Fluids 37 (2006) 209–214.
[50] J.B.M. Goodall, S. Kellici, D. Illsley, R. Lines, J.C. Knowles, J.A. Darr, RSC Adv. 4 (2014) 31799–31809.
[51] V. Middelkoop, C.J. Tighe, S. Kellici, R.I. Gruar, J.M. Perkins, S.D.M. Jacques, P. Barnes, J.A. Darr, J. Supercrit. Fluids 87 (2014) 118–128.
[52] Y. Liang, H. Wang, H.S. Casalongue, Z. Chen, H. Dai, Nano Res. 3 (2010) 701–705.
[53] J. Su, M. Cao, L. Ren, C. Hu, J. Phys. Chem. C 115 (2011) 14469–14477.
[54] S.D. Perera, R.G. Mariano, K. Vu, N. Nour, O. Seitz, Y. Chabal, K.J. Balkus Jr., ACS Catal. 2 (2012) 949–956.
[55] N. Li, M. Zheng, X. Chang, G. Ji, H. Lu, L. Xue, L. Pan, J. Cao, J. Sol. State Chem. 184 (2011) 953–958.
[56] S. Kellici, K.A. Gong, T.A. Lin, S. Brown, R.J.H. Clark, M. Vickers, J.K. Cockcroft, V. Middelkoop, P. Barnes, J.M. Perkins, C.J. Tighe, J.A. Darr, Philos. Trans. A: Math. Phys. Eng. Sci. 368 (2010) 433–4349.
[57] T. Lin, S. Kellici, K. Gong, K. Thompson, J.R.G. Evans, X. Wang, J.A. Darr, J. Comb. Chem. 12 (2010) 383–392.
[58] W.S. Hummers, R.E. Offeman, J. Am. Chem. Soc. 80 (1958) 1339.
[59] Y.W. Zhu, S. Murali, W.W. Cai, X.S. Li, J.W. Suk, J.R. Potts, R.S. Ruoff, Adv. Mater. 22 (2010) 5226.
[60] D.C. Marcano, D.V. Kosynkin, J.M. Berlin, A. Sinitskii, Z.Z. Sun, A. Slesarev, L.B. Alemany, W. Lu, J.M. Tour, ACS Nano 4 (2010) 4806–4814.
[61] X.L. Weng, P. Boldrin, I. Abrahams, S.J. Skinner, S. Kellici, J.A. Darr, J. Solid State Chem. 181 (2008) 1123–1132.
[62] Z. Zhang, S. Brown, J.B.M. Goodall, X. Weng, K. Thompson, K. Gong, S. Kellici, R.J.H. Clark, J.R.G. Evans, J.A. Darr, J. Alloy. Compd. 476 (2009) 451–456.
[63] S. Kellici, J. Acord, J. Ball, H.S. Reehal, D. Morgan, B. Saha, RSC Adv. 4 (2014) 14858–14861.
[64] A. Cabanas, J. Darr, E. Lester, M. Poliakoff, J. Mater. Chem. 11 (2001) 561–568.
[65] A. Cabanas, J. Darr, E. Lester, M. Poliakoff, Chem. Commun. 11 (2000) 901–902.
[66] X. Weng, B. Perston, X. Wang, I. Abrahams, T. Lin, S. Yang, J. Evans, D. Morgan, A. Carley, M. Bowker, J. Knowles, I. Rehman, J. Darr, Appl. Catal. B: Environ. 90 (2009) 405–415.
[67] T. Pirmohamed, J.M. Dowding, S. Singh, B. Wasserman, E. Heckert, A.S. Karakoti, J.E.S. King, S. Seal, W.T. Self, Chem. Commun. 46 (2010) 2736–2738.
[68] E.J. Preisler, O.J. Marsh, R.A. Beach, T.C. McGill, J. Vac. Sci. Technol. B 19 (2001) 1611–1618.
[69] Z. Tan, S. Li, F. Wang, D. Qian, J. Lin, J. Hou, Y. Li, Sci. Rep. 4 (2014) 4691.
[70] K. Tomishige, H. Yasuda, Y. Yoshida, M. Nurunnabi, B. Li, K. Kunimori, Green Chem. 5 (2004) 206–214.
[71] M. Tamura, M. Honda, Y. Nakagawa, K. Tomishige, Catal. Sci. Technol. 89 (2014) 19–33.
[72] Y. Lilach, I. Danziger, M. Asscher, Catal. Lett. 76 (2001) 35–39.
[73] S. Navalon, A. Dhakshinamoorthy, M. Alvaro, H. Garcia, Chem. Rev. 114 (2014) 6179–6212.
[74] M. Cutrufello, I. Ferino, V. Solinas, A. Primavera, A. Trovarelli, A. Auroux, C. Picciau, Phys. Chem. Chem. Phys. 1 (1999) 3369–3375.
[75] J. Bian, M. Xiao, S. Wang, X. Wang, Y. Lu, Y. Meng, Chem. Eng. J. 147 (2009) 287–296.
[76] S. Anderson, S. Manthata, T. Root, Catal. A: Gen. 280 (2005) 117–124.
[77] T. Zhao, Y. Han, Y. Sun, Fuel Process. Technol. 62 (2000) 187–194.
[78] Y. Cao, H. Cheng, L. Ma, F. Liu, Z. Liu, Catal. Surv. Asia 16 (2012) 138–147.
[79] F. Cao, D. Fang, D. Liu, W. Ying, Fuel Chem. Div. Reprints 74 (2002) 295–297.
[80] J. Wang, X. Yue, F. Cai, L. He, Catal. Commun. 8 (2007) 167–172.
[81] Y. Du, F. Cai, D. King, L. He, Green Chem. 7 (2005) 518–523.
[82] A. Baiker, Chem. Rev. 99 (1999) 453–473.